2023-01-1423 Published 15 Jun 2023

# Comparability of Hot-Wire Estimates of Liquid Water Content in SLD Conditions

**Biagio M. Esposito** CIRA Scpa

**David Orchard** National Research Council Canada

**Johannes Lucke** Deutsches Zentrum fur Luft und Raumfahrt

**Leonid Nichman and Natalia Bliankinshtein** National Research Council Canada

**Lyle Lilie** Science Engineering Associates Inc

**Pietro Catalano and Francesco D'Aniello** CIRA Scpa

**J. Walter Strapp** Met Analytics Inc.

***Citation:*** Esposito, B.M., Orchard, D., Lucke, J., Nichman, L. et al., "Comparability of Hot-Wire Estimates of Liquid Water Content in SLD Conditions," SAE Technical Paper 2023-01-1423, 2023, doi:10.4271/2023-01-1423.

Received: 30 Nov 2022 Revised: 07 Apr 2023 Accepted: 26 Apr 2023

## Abstract

Future compliance to FAA 14 CFR Part 25 and EASA CS-25 Appendix O conditions has required icing wind tunnels to expand their cloud simulation envelope, and demonstrate accurate calibration of liquid water content and droplet particle size distributions under these conditions. This has led to a renewed community interest in the accuracy of these calibrations, and the potential inter-facility bias due to the choice of instrumentation and processing methods. This article provides a comparison of the response of various hot-wire liquid water content instruments under Appendix C and supercooled large droplet conditions, after an independent similar analysis at other wind tunnel facilities. The instruments are being used, or are under consideration for use, by facilities collaborating in the ICE GENESIS program. For droplet median volume diameters (MVDs) between about 15 and 250 µm, cylindrical hot wire LWC sensors were found to consistently and increasingly under-read measurements from conical and trough TWC sensors as MVD increased, and were not considered further. Of the remaining TWC sensors, the specific instruments investigated were found to agree within about ± 20% of their average test point response for the range of conditions tested, but systematic scale differences between instruments were found to reach about a factor of 1.4. Sensitivity to increasing droplet MVD was concluded to be similar amongst different instruments given the uncertainties, except for two that exhibited notable roll-off with MVD relative to the others.

## Introduction

Various technologies for cloud liquid water content (LWC) measurement have been developed over the years, including optical devices, evaporative devices using differential hygrometry ("evaporators"), and hot-wires, also evaporative devices but commonly deducing LWC by measuring the power required to keep an exposed wire at a constant temperature. The hot-wire device is commonly used for airborne and wind tunnel measurements, primarily due to its relatively small size, and simplicity of operation and data processing. A number of wind tunnel studies have been published over the years documenting the response of hot-wires under both liquid and ice conditions. The response of cylindrical hot-wires has been long known to roll off with increasing MVD (e.g. [1,2]), whereas the response of hot-wire sensors with a capture-volume (e.g. troughs, cones), typically referred to as total water content (TWC) sensors, has been found to be more flat with increasing MVD relative to tunnel reference values. Due to the current emphasis on calibration in SLD conditions, the interest has turned to the use of TWC hot-wires for LWC calibration. A more complete description of cloud water content measuring devices can be found in Refs. [3, 4]. Comparisons of LWC response of hot-wire cylindrical and trough or cone sensors can be found in [2, 5, 6, 7]. In the main body of this article we will restrict the discussion to the response of TWC sensors, due to their superior efficiency in higher MVD conditions. Appendix B summarizes the cylindrical sensor measurements for documentation.

In the past, icing wind tunnels have typically produced calibrated cloud simulations within the Appendix C envelope, nominally varying in droplet MVD between about 10 µm and 30 µm. Cloud LWC was usually estimated by ice accretion methods, such as a rotating cylinder [8] or an icing blade [9]. Errors in LWC determined using these methods was estimated by the above authors to be less than 10% and perhaps to within a few percent. As these facilities have expanded their envelopes to include SLD conditions, and as comparisons to measurements from hot-wires and other devices have become available, it has become evident that traditional ice accretion calibration methods and existing tunnel reference LWCs may not be sufficiently accurate in high-MVD situations. For example, the rotating icing cylinder technique has been used at the National Research Council (NRC) of Canada Altitude Icing Wind Tunnel (AIWT), and its calibration has been compared to the Science Engineering Associates (SEA) Multi-Element Water Content System [5], hereafter referred to as the multi wire (MW) probe, where the tunnel calibration at high MVD appeared to be underreading [10, 7]. Similarly, in the past the National Aeronautics and Space Administration (NASA) Icing Research Tunnel (IRT) performed LWC calibrations in both Appendix C and supercooled large droplet (SLD) conditions with an icing blade and a large cylinder. Within the last decade, the IRT has changed to using a MW TWC sensor for LWC calibration, after establishing its agreement with the icing blade in Appendix C conditions, and its apparently superior performance in high MVD conditions [6]. The accuracy of wind tunnel LWC calibrations via ice accretion methods in SLD conditions, and the validity of using them as reference values for assessing instrument accuracy is arguably open for debate. Furthermore, LWC calibration using such methods is laborious and time consuming, and as increased information on the relative performance of ice accretion and LWC-measuring instruments has become available, the practical advantages of instrument measurements have made their use an attractive calibration alternative.

The ICE GENESIS community is interested in understanding the response of the different instruments being used for LWC calibration by its participating icing wind tunnels. Such information is required to estimate inter-facility bias for ICE GENESIS experiments run in these facilities, as well as to work towards absolute LWC uncertainty estimates. The instruments that have been used for LWC calibration include the SEA MW [5], the SkyPhysTech Inc. Nevzorov probe [11], and the Cranfield University isokinetic evaporator. A detailed study of the comparability of these devices has been provided by [12]. In the current study, independent measurements with some of the same devices is presented using data collection in a different wind tunnel facility, the NRC AIWT. The Centro Italiano Richerche Aerospaziale (CIRA) icing wind tunnel has recently been upgraded with a new nozzle system and the instrument comparisons shown in this article were motivated by the search for a suitable SLD LWC calibration probe for their configuration.

In September, 2020, a five-day wind tunnel test of various hot-wires used by ICE GENESIS partners was conducted at the NRC AIWT in Ottawa, Canada. Tunnel time was provided by the NRC as part of the CIRA collaboration. Although the NRC measurements shared common AIWT test points with the North American led SLD Instrumentation Collaboration study [13], the current effort focused on instruments currently used or proposed for tunnel calibration in the ICE GENESIS project. In the following sections, comparisons of this study's hot-wire measurements over a wide range of MVDs are provided.

# Test Description

The testing was performed over five days of measurements at the NRC AIWT in September 2020. The AIWT is a closed-circuit wind tunnel that can be operated between 5 and 100 $ms^{-1}$ with the standard working section used for these tests. The nominal LWC and MVD ranges are 0.1 to 2.5 $gm^{-3}$, and 8 to 200 µm, although MVDs as high as 250 µm were tested. A more detailed description of the tunnel and its capabilities can be found in [7].

## Instruments

The instruments tested at the NRC AIWT included the following:

- Nevzorov system (standard 8 mm cone and non-standard 12 mm cone), Sensor Serial Number (SSN) 416, provided by the German Aerospace Center (DLR), Figure 1.
- SEA MW (long strut version), SSN 2086, provided by CIRA, Figure 2.
- Nevzorov system (standard 8 mm cone), SSN 300, provided by NRC Flight Research Laboratory (FRL), Figure 3
- SEA Ice Crystal Detector (ICD), [14], SSN 4005, provided by NRC FRL, Figure 4
- SEA Robust Probe [15], SSN 3010, provided by CIRA, Figure 5

Table 1 shows the dimensions of the each of the TWC sensor elements, and the sensor identifier that will be used

**FIGURE 1** Drawing of Nevzorov SSN 416 with 8 and 12 mm cones, used to provide the" N8mm416" and "N12mm416" results of this study. From [12].

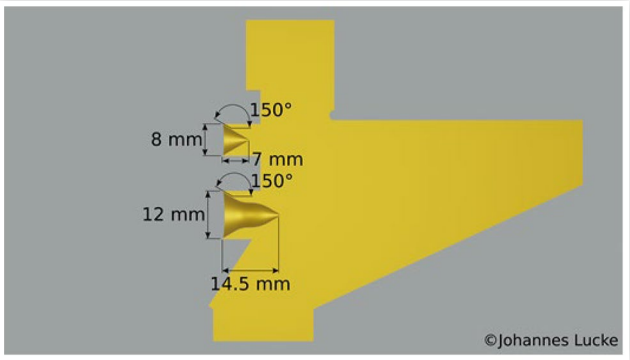

**FIGURE 2** SEA Multi-element probe, or "multi-wire (MW)", with 0.53 mm cylindrical wire (left), 2.11 mm trough TWC sensor (center), and 2.11 mm cylindrical sensor (right). The TWC sensor was used to provide the "MWTWC" results of this study. From [6].

**FIGURE 3** Standard Nevzorov and sensor vane with 8 mm TWC cone, as used to provide the N8mm300 sensor results of this study.

below when discussing results. It is sensible to expect that the retention efficiency of the elements could be affected by the sensor characteristics, particularly for large droplets that may splash on impact. The 12 mm Nevzorov cone sensor was specifically designed to enhance large particle capture and evaporation, with its deep interior collection cavity.

**FIGURE 4** SEA Ice Crystal Detector, from [14]. The concave sensor provided the "ICDTWC" results used in this study.

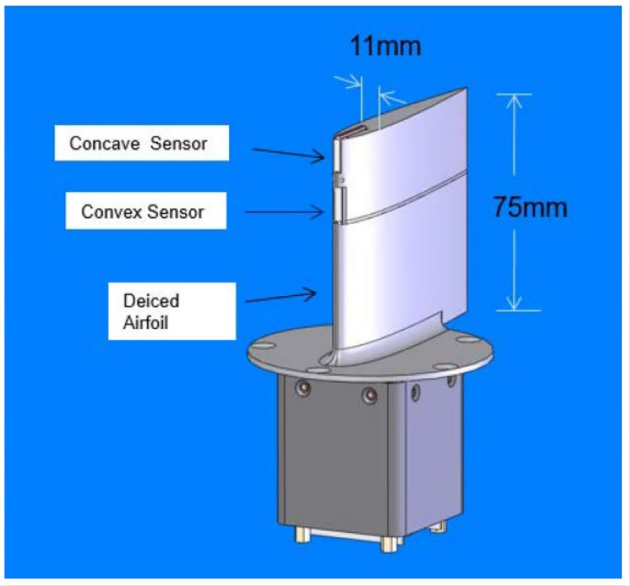


**FIGURE 5** SEA Robust probe, from [15], used to provide the "ROBTWC" results of this study

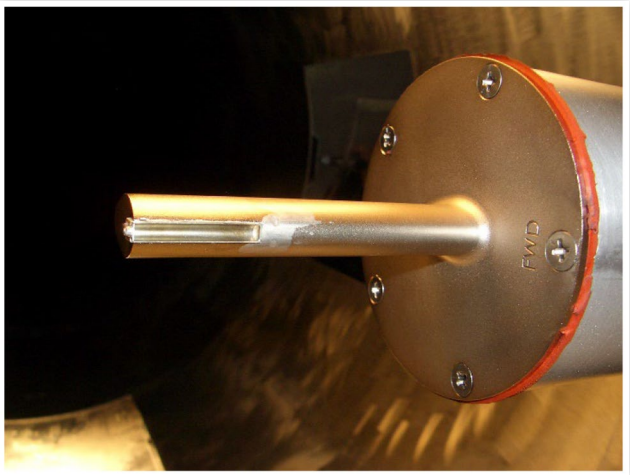


For all tests, the NRC Spraytec Ind. Malvern laser diffraction particle size system was used to estimate the droplet relative volume distribution and MVD. Measurements were made unobtrusively with the transmit and receive optics mounted outside the tunnel during each test point. MVDs provided in this article are from a facility real time parameterization of MVD as a function of nozzle and tunnel parameters.

The MW, ICD, and Nevzorovs also include separate cylindrical wires in addition to the TWC wires. In order to simplify the content of the main body of this article, cylindrical sensor measurements have been separately summarized in Appendix B. Due to their decreasing response with increasing MVD relative to TWC sensors, they were concluded to be inferior in SLD conditions. Therefore, only results from the TWC wires from each of these sensors will be summarized below.

**TABLE 1** Width (W) or diameter (D), length (L), sample area (SA), and depth of TWC sensing elements in this study

| Sensor | Identifier | W or D (mm) | L (mm) | SA ($mm^2$) | Depth (mm) |
|---|---|---|---|---|---|
| Nevorov conical 12 mm TWC sensor, SSN 416 | N12mm416 | 12.1 | n/a | 114.9 | 14.5 |
| Nevorov conical 8 mm TWC sensor, SSN 416 | N8mm416 | 8.1 | n/a | 51.5 | ~6.9 |
| Nevorov conical 8 mm TWC sensor, SSN 300 | N8mm300 | 8.0 | n/a | 50.2 | ~6 |
| SEA Multiwire TWC sensor, SSN 2086 | MWTWC | 2.11 | 22.81 | 48.1 | 0.86 |
| SEA ICD TWC sensor, SSN 4005 | ICDTWC | 2.41 | 10.21 | 24.6 | 1.09 |
| SEA Robust TWC sensor, SSN 3010 | ROBTWC | 3.6 | 22.94 | 82.5 | 1.57 |

## Test Plan

The standard AIWT working section used for these tests was 57 cm high, by 57 cm wide, by 183 cm long. The height and width allowed for multiple sensors to be mounted simultaneously around the center point of the tunnel. However, as reported in [7], due to the distribution of LWC away from the center, and possible aerodynamic interference between simultaneously mounted instruments, potentially complex corrections could be required for different sensor locations. Consequently, it was decided to test each probe by itself with its sample volume at the center point of the tunnel, and take advantage of the high level of repeatability of the tunnel, which will be demonstrated in the results section. However, the N12mm416 and N8mm416 measurements were taken simultaneously, with the N8mm416 sensor at the tunnel center, and the N12mm416 sensor approximately 22 mm lower than the center (Figure 1).

The test points are summarized in Tables 2 and 3. First there were two "MVD Sweeps", one at 80 $ms^{-1}$ and the other at 100 $ms^{-1}$. The LWC was set to nominal tunnel calibrated values of 0.5 $gm^{-3}$ and 0.2 $gm^{-3}$ respectively, and the MVD was varied in individual test points between approximately 15 and 250 µm, and 30 and 235 µm MVD respectively. As discussed in [10, 7], the NRC tunnel nominal LWCs at high MVD varied significantly from the measured hot-wire LWCs, so the MVD Sweeps likely contained both an LWC and TWC variation. Nevertheless, conditions should have been the same for each instrument. Second, there were three "LWC Sweeps", all at 80 $ms^{-1}$, where the MVD was kept constant at 20, 100, or 250 µm MVD, and the LWC was varied as per tunnel practical limits. For each test point, the actual sampling accomplished for each sensor is identified under individual columns in Tables 2 and 3. There are two columns for the ROBTWC. ROBTWC (2) refers to measurements taken at the tunnel center, and ROBTWC (1) refers to additional measurements taken approximately 3.8 cm below the tunnel center. For comparison to other instruments, only ROBTWC measurements at the center are included in this article. Unfortunately, due to time constraints, only a partial matrix could be completed for the ROBTWC at the tunnel center. The comparison of ROBTWC (1) and ROBTWC (2) were however useful in identifying a vertical gradient of TWC near the tunnel center. Four additional points not included in Tables 2 and 3 were also tested for miscellaneous purposes, but are not central to this study, and will not be discussed further.

**TABLE 2** Test points for MVD Sweeps at 80 $ms^{-1}$ and LWC of 0.5 $gm^{-3}$ (upper), and 100 $ms^{-1}$ and 0.2 $gm^{-3}$ (lower).

| Type | Nom LWC | Nom MVD | N12mm416, N8mm416 | N8mm300 | MW TWC | ICDTWC | ROBTWC (1) | ROBTWC (2) |
|---|---|---|---|---|---|---|---|---|
| **MVD Sweep~0.5 $gm^{-3}$ 0 $ms^{-1}$** | 0.5 | 15 | 1x | 2x | 1x | 1x | 1x | |
| | 0.5 | 20 | 5x | 2x | 7x | 1x | 6x | 1x |
| | 0.5 | 28 | 1x | 1x | 1x | 1x | 1x | |
| | 0.5 | 40 | 1x | 1x | 1x | 1x | 1x | |
| | 0.5 | 50 | 1x | 1x | 1x | 1x | 1x | 1x |
| | 0.5 | 57 | 5x | 1x | 6x | 1x | 5x | 1x |
| | 0.5 | 78 | 1x | 1x | 1x | 1x | 1x | 1x |
| | 0.5 | 100 | 4x | 1x | 5x | 1x | 5x | 6x |
| | 0.5 | 125 | 1x | 1x | 1x | 1x | 1x | 1x |
| | 0.5 | 175 | 1x | 1x | 1x | 1x | 2x | 1x |
| | 0.5 | 210 | 1 x | 1x | | | 1x | 1x |
| | 0.5 | 230 | 5x | 2x | 5x | 1x | 5x | 6x |
| | 0.5 | 250 | 1x | | 1x | 1x | 1x | 1x |
| **MVD Sweep ~0.2 $gm^{-3}$ 100 $ms^{-1}$** | 0.2 | 30 | 1x | 1x | 2x | 3x | 1x | |
| | 0.2 | 180 | 1x | 1x | 2x | 1x | 2x | 1x |
| | 0.2 | 240 | 1x | 1x | 1x | 1x | 1x | 1x |

The "nx" in each column identifies which instruments were tested for a particular test point, and how many times. ROBTWC(1) and ROBTWC(2) were measured 3.8 cm below and at the tunnel center respectively. See text for description of probes. LWCs and MVDs are tunnel calibrated nominal values.

**TABLE 3** As in Table 1, but for LWC Sweeps at 80 ms-1, 20 μm (upper), 100 μm (middle), and 250 μm tunnel MVD (lower)

| Type | Nom LWC | Nom MVD | N12mm416, N8mm416 | N8mm300 | MW WC | ICDTWC | ROBTWC (1) | ROBTWC (2) |
|---|---|---|---|---|---|---|---|---|
| **LWC sweep 80 ms$^{-1}$ ~20 μm** | 0.5 | 20 | 5x | 2x | 7x | 1x | 6x | 1x |
| | 1 | 20 | 1x | 3x | 1x | 1x | 1x | |
| | 1.5 | 20 | 1x | 3x | 1x | 1x | 1x | |
| | 2 | 20 | 5x | 1x | 6x | 1x | 5x | 1x |
| | 2.5 | 20 | 1x | 1x | 1x | 1x | 1x | |
| | 3 | 20 | 1x | 1x | 1x | 1x | 1x | |
| **LWC sweep 80 ms$^{-1}$ ~100 μm** | 0.25 | 100 | 1x | 2x | 1x | 1x | 1x | 1x |
| | 0.5 | 100 | 4x | 1x | 5x | 1x | 5x | 6x |
| | 0.75 | 100 | 1x | 1x | 1x | 1x | 1x | 1x |
| | 1 | 100 | 1x | 1x | 1x | 1x | 1x | 1x |
| **LWC sweep 80 ms$^{-1}$ ~250 μm** | 0.25 | 250 | 2x | 2x | 1x | 1x | 1x | 1x |
| | 0.5 | 250 | 5x | 1x | 5x | 1x | 5x | 6x |
| | 0.75 | 250 | 1x | 1x | 1x | 1x | 2x | 1x |
| | 1 | 250 | 1x | 1x | 1x | 1x | 1x | 1x |

Finally, a series of previously untested bi-modal test points was run on the final day, but were not included due to the absence of PSD information at the time of writing of this article. The PSDs of all test points included in this article were fundamentally unimodal.

## LWC Calculation

Since all hot-wires of this study were operated at constant temperature, it was possible to use the same LWC calculation algorithm for each. The basic equations have been summarized elsewhere: e.g. see Ref. [3], equation 3.2; [4] equation 6.3.2; [6], equation 2, where further discussion of the calculations can also be found. For this study, the same basic formulae were used in the same manner for each instrument. Three of the sensors (N12mm 416, N8mm416, N8mm300, and MWTWC) included additional reference wires that are designed to provide an estimate of the dry power in cloud, which must be subtracted from the total power to derive LWC. Based on past experience, it was decided to not use the data from these reference wires. For the MWTWC, it had been previously found by one of the co-authors of this study that the LWC calculation could be decreased by up to 4% by what was thought to be wetting or some other in-cloud influence on the reference wire. This conclusion was supported by similar investigations detailed in [6]. For the Nevzorov sensors, there was generally no specific indication of a false deflection of the reference wire in cloud, except when icing on the sensor vane during some of the higher LWC runs caused differential drift between the TWC and reference sensors, resulting in unnecessary LWC uncertainty. This icing has also been noted in [16] from analysis of the same dataset, where more detail can be found. For these reasons, the in-cloud dry term for all sensors was estimated by implementing a Nu-Re dry term parameterization, fit during the dry periods of sensor exposure during the tests. These parameterizations typically resulted in LWC calculations of ±0.02 gm$^{-3}$ out of cloud, which was persistent and could drift somewhat with time. A manual subtraction was used as a final minor correction to remove these zero LWC offsets. It is expected that use of the reference wires for the dry term would have had only a minor effect on results.

The inertial collision efficiencies for these sensors are summarized in Appendix A, where a Table A1 summarizes various efficiencies at the approximate test point MVDs. Note that these collision efficiencies describe the impingement of water droplets due to their inertia, drag, and interaction with the aerodynamic flow field. They do not include splashing and re-entrainment of droplets impacting the sensor, which can dominate net sensor efficiency. This latter effect has not been well characterized for TWC sensors, and is in one of the main effects that could affect inter- instrument variability in SLD conditions. The origins of the inertial collision efficiencies of Appendix A are quite varied and there is a lack of consistency in approach. In a few cases, more than one algorithm was available. For the ICDTWC, there was no algorithm available, and collision efficiencies were assumed to be 1.0. All efficiencies derived from algorithms, with the exception of the N12mm416, were above 0.95 for MVDs larger than 50 μm, and thus collision efficiency uncertainty likely did not contribute significantly to inter-instrument variability in the high-MVD SLD conditions. But for lower MVDs, discrepancies increased, even between two efficiency algorithm options for the same sensor (e.g. a 0.1 difference between the two options for the Robust TWC efficiency at 20 μm MVD). The lowest efficiencies were for the N12mm416 (e.g. 0.346 at 15 μm MVD, 0.832 at 50 μm MVD, and it is therefore prudent to apply more uncertainty to these values. All collision efficiencies were applied at the MVD value of the test point, approximated by real-time measurements of tunnel parameters that have been calibrated using the Malvern to provide test-time MVDs. The one exception was for the N12mm416, which was applied at the effective diameter $d_{eff}$ as required by the algorithm. See Appendix A for details. Appendix A also includes an estimate of the effect of calculating efficiencies at the MVD rather than discretely over the entire PSD. For MVDs larger than 50 μm, the PSD-derived net efficiency was always lower than the MVD efficiency, but at most about 1%

**FIGURE 6** Example set of test point time history from this study.

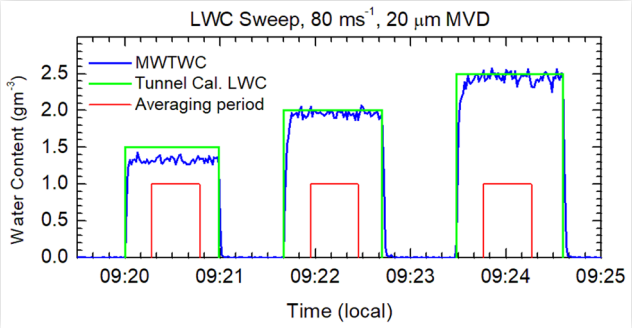


below. For MVDs less than 50 μm, the PSD efficiency reached about 4% lower than the MVD efficiency. No corrections for this effect have been applied herein. Further, no such assessment was required for the N12mm416 since its formulation was dependent only on the bulk parameter $d_{eff}$.

Figure 6 illustrates a typical sequence of test points, shown here for the MWTWC during this study. Although this example displays 60 second tests, a 120 second duration was more typically performed, with gaps of about 30-60 seconds between tests. In this figure, the nominal NRC calibration set-point LWC is shown as the green line, the period of averaging the red line, and blue line is the MWTWC trace, at this point uncorrected for collision efficiency. The averaging period was usually chosen to exclude the first and last 15 seconds of the spray. Each period was examined visually for spray irregularities, and averaging periods and durations were occasionally modified accordingly. Collision efficiency corrections were applied as a last step after averaging.

# Results

## Tunnel Repeatability

The validity of comparing non-simultaneous measurements in this study is dependent on the repeatability of the tunnel for the same test conditions. A series of repeats were performed for each instrument, and the standard deviations of the measurements are summarized in Table 4. Repeats were not performed for all test points due to available time. When performed, the number of repeats for a given test point per instrument varied between two and seven, and only cases of four or more repeats are summarized in the table. It is important to note that variations indicated by the table can include both tunnel repeatability and instrument precision, and the results should be used only as a general guideline in assessing inter-instrument differences in the following sections. In general, the standard deviation of repeats increased with LWC, and there is some indication of higher spread at the higher MVDs. The ±2σ values varied between about ±0.004 gm$^{-3}$ and ±0.10 gm$^{-3}$. The coefficient of variation varied between about 1% and 6%, the highest values being at the highest MVDs.

## Effect of Mounting Location

The sampling of the ROBTWC at the center and additionally 3.8 cm below the center was important in identifying an apparent vertical gradient of LWC near the tunnel center. For example, Figure 7 shows comparisons of the two locations for the 100 μm LWC Sweep. The measurements at the two locations were highly correlated with the below-center

**FIGURE 7** Comparison of ROBTWC measurements 3.8 cm below center, to ROBTWC measurements at the tunnel center, illustrating vertical LWC gradient in tunnel; for LWC Sweep at 100 μm MVD.

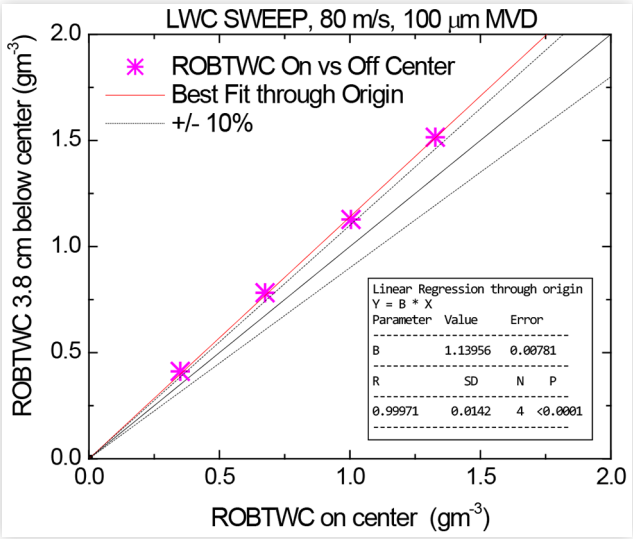


**TABLE 4** Standard deviation (σ) of spray-average LWCs measured by each sensor for sprays with at least four repeats. There were no such cases for N8mm300 or ICDTWC. See Tables 2 and 3 for the number of repeats.

| Nom LWC g/m3 | Nom MVD μm | MWTWC σ g/m3 | N12mm416 σ g/m3 | N8mm416 σ g/m3 | ROB TWC σ off cent. g/m3 | ROBTWC σ on cent. g/m3 | All g/m3 |
|---|---|---|---|---|---|---|---|
| 0.5 | 20 | 0.010 | 0.005 | 0.006 | 0.004 | | 0.007 |
| 2.0 | 20 | 0.015 | 0.019 | 0.052 | 0.013 | | 0.028 |
| 0.5 | 57 | 0.005 | 0.007 | 0.008 | 0.005 | | 0.006 |
| 0.5 | 100 | 0.007 | 0.004 | 0.002 | 0.028 | 0.005 | 0.014 |
| 0.5 | 230 | 0.031 | 0.004 | 0.012 | 0.024 | 0.008 | 0.018 |
| All | | 0.015 | 0.010 | 0.025 | 0.017 | 0.007 | |

measurement approximately a factor of 1.14 of the center measurement. Corresponding ratios for the 20 and 230 μm LWC Sweeps were 1.053 and 1.106 respectively. The only sensor not mounted at the center of the tunnel, at 2.2 cm below center, was N12mm416, because it was taken simultaneously with its N8mm416 sensor. This will be discussed again later in context of the following results.

## LWC Sweeps at Constant Tunnel MVD

In the following sections, comparisons will be made between the various instruments for the MVD and LWC sweeps summarized in Tables 2 and 3. Comparisons to the tunnel LWC were generally not used, as there was a common observation from all instruments of lower tunnel readings as MVD increased, which complicated inter-instrument comparisons. This has been discussed further in [7] and [10]. In Figures 8–12 the average response of all hot-wires at a particular test point has alternatively been chosen as a reference. It is contended here that this choice better quantifies the average inter-facility uncertainty caused by the use of different hot-wire calibration devices. For each test point, repeats were averaged, and then a single value from each sensor was used to produce the all-instrument-average, so as not to bias averages to an instrument that had repeats. Eight of the thirty test points of Tables 2 and 3 did not have measurements from all sensors, and in those cases a simple average of the available instruments was used to produce the all-instrument-average. This could produce some bias for these particular test points, but did not appreciably affect the overall conclusions of this study. Note that results close to the one-to-one line in Figures 8–12 are not necessarily more accurate results. They are just closer to the average of all instruments. For Figures 8–10, due to linear regressions usually having small intercepts, regression slopes through the origin have been used to express approximate scale factor differences between probe measurements.

**FIGURE 8** Comparison of hot-wire instrument response, relative to the average LWC measured by all instruments, for the LWC Sweep at 80 ms-1 and 100 μm MVD.

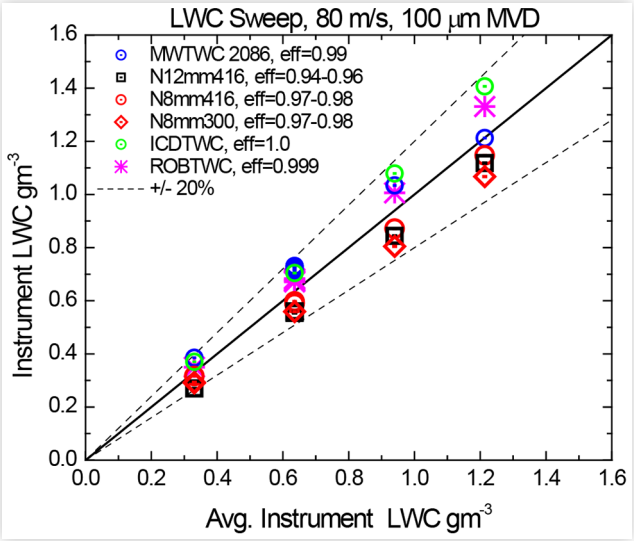


**FIGURE 9** As in Fig. 8, but for the LWC Sweep at 80 ms-1 and 230 μm MVD

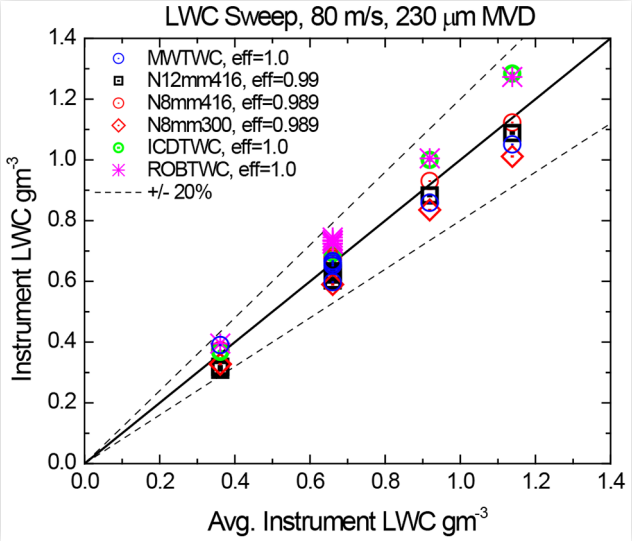


**FIGURE 10** As in Fig. 8, but for the LWC Sweep at 80 ms-1 and 20 μm MVD

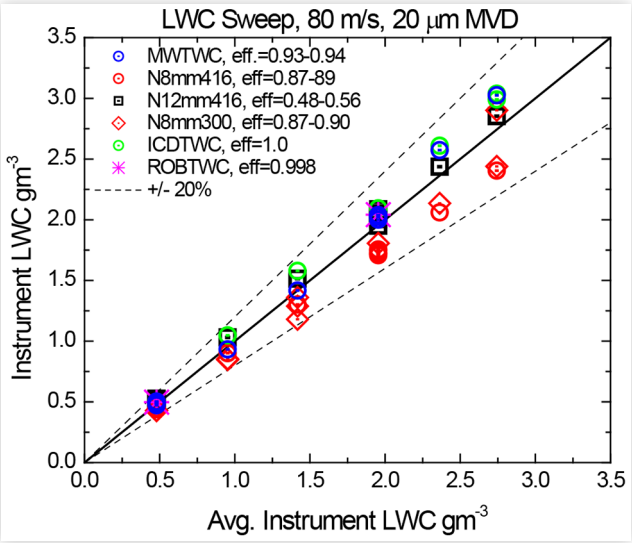


Figure 8 shows hot-wire TWC comparisons for the LWC Sweep at 80 ms-1 and 100 μm MVD. At this MVD, inertial collision efficiencies were all greater than 0.95, so efficiency uncertainty did not likely to contribute greatly to differences. Repeats are included in this figure, and are difficult to distinguish due to their similarity. For example, the N12mm416, N8mm416, and MWTWC, and ROBTWC all had four or more repeats for the abscissa value of 0.64 gm-3. All instrument results were contained within ±20% of the average values, although systematic differences were observed. All results increased more or less linearly with increasing average LWC, with the exception of the MWTWC, which displayed some roll-off for the highest LWC point. However, this was based

**FIGURE 11** Results of MVD Sweep at tunnel calibrated LWC of 0.5 gm$^{-3}$, and 80 ms$^{-1}$: ratio of measured hot-wire LWC, to average of all hot-wire LWCs at a given MVD, as a function of tunnel calibration MVD. Low-MVD N12mm416 points should be disregarded due to no collision efficiency correction

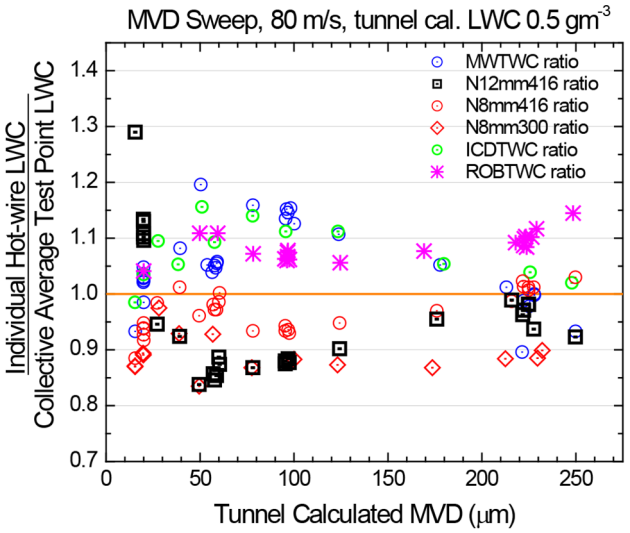


**FIGURE 12** As in Fig. 11, but for the MVD Sweep at 100 ms-$^{1}$, and tunnel calibration LWC of 0.2 gm-$^{3}$.

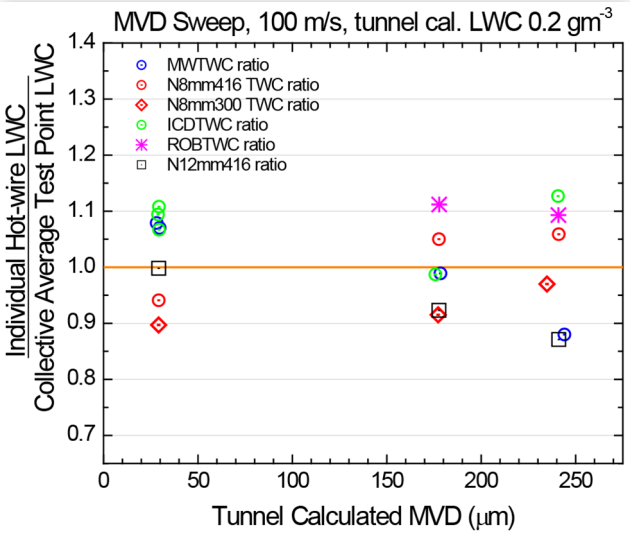


on a single MWTWC point, which may be an outlier. All Nevzorov results were typically lower than the MWTWC, ICDTWC, and ROBTWC. The ratio of the regression slopes between the highest response sensor (ICDTWC) and the lowest (N8mm300) yielded a scale difference of 1.31. The N8mm416 and N8mm300 (red circles and red diamonds), were similar, the former being about a factor of 1.073 higher according to the regression slopes. The N12mm416 and N8mm416 values were highly correlated and nearly identical, although there is some uncertainty due to the N12mm416 being below the tunnel center, and possibly in a higher LWC zone due to the observed vertical gradient discussed earlier.

Figure 9 shows the comparisons for the LWC sweep at 80 ms$^{-1}$ and 230 μm MVD. Again, all collision efficiencies were greater than about 0.99. All instruments exhibited an approximate linear response with respect to the collective average hot wire LWC, except for the MWTWC, which continued to show a roll off relative to other probes with increasing LWC. As before, all measurements were contained within ±20% of the average response, and systematic differences were observed between instruments. All the Nevzorov results were similar to each other and lower than the ICDTWC and ROBTWC, which in turn were also quite similar. Comparing the ICDTWC and the N8mm300, the ratio of the regression slopes suggested a scale difference of about 1.22, a decrease from the 1.31 scale ratio observed in the 100 μm MVD sweep. More difference was observed between N8mm416 and N8mm300 (regression slope ratio of 1.13). The N8mm416 now read a little higher than the N12mm416, even at this high MVD, with a regression slope ratio of 1.07. This was in spite of the fact that the tunnel LWC may have been higher at the lower position of the N12mm416.

Figure 10 shows the results of the LWC sweep at 80 ms$^{-1}$ and 20 μm MVD. In this case, inertial collision efficiencies were expected to be more important. The values used are included in the figure legend. The present lack of efficiencies for ICDTWC, which was set to unity for this study pending the completion of CIRA CFD analysis, likely means that ICD results were underestimates. Only two test points were performed for the ROBTWC at the tunnel center, so interpretation of its results was limited. Once again, all measurements were well within ±20% of the average response, and systematic differences were observed between instruments. The ICDTWC yielded the highest results, and the Nevzorov 8 mm results were again usually lower than the average. However, inter-instrument differences were collectively smaller at this MVD. Between the highest response instrument (ICDTWC) and the lowest (N8mm300), the ratio of regression slopes yielded a scale difference of 1.23. The two Nevzorov 8mm cones provided nearly identical regression slopes. The N12mm416 results were about a factor 1.04 above the average line for all measurements, and about a factor 1.05 lower than the ICDTWC. Its measurements were highly correlated to N8mm416, with the former about a factor of 1.17 higher. The N12mm416 had a quite low estimated efficiency of 0.56, and perhaps more uncertainty due to the corresponding larger correction. Furthermore, it was potentially in a higher LWC zone due to apparent tunnel vertical gradient in LWC

One final comparison is made to the AIWT tunnel LWC calibration equations. At this MVD, the calibration is based on 2.4 mm diameter rotating cylinder measurements. The 20 μm MVD is a commonly used test point for Appendix C conditions, and the general belief has been that rotating cylinder and icing blade measurements do not suffer from underestimation due to splashing at this MVD, and LWC estimates are likely better than 10%. For editorial economy, only regression slopes through the origin of instrument LWC versus tunnel calibration LWC are provided here, as follows: MWTWC 1.008; N8mm416 0.847; N12mm416 0.995; N8mm300 0.847; ICDTWC 1.026; ROBTWC 1.019. There was a slight bias in pre-test icing cylinder checks at 20 μm, yielding a corresponding slope of 1.038 relative to the tunnel equations. The icing cylinder measurements and tunnel equations were

higher than the average instrument response, and very close to the ICDTWC.

## MVD Sweeps at Constant Tunnel LWC

The next series of comparison are for the MVD sweeps. The main focus on these comparisons will be on the higher MVD test points, where inertial collision efficiencies approached unity, and thus results are less subject to uncertainty.

Figure 11 shows the results of the MVD Sweep at 80 $ms^{-1}$ at a tunnel calibrated LWC of 0.5 $gm^{-3}$. As discussed in [10, 7], there is evidence that the tunnel LWC calibration, using rotating cylinders of different diameters, likely underestimated the LWC at higher MVD values. The ratios of the individual hot wire LWCs to the collective average LWCs from all hot-wire devices are shown plotted versus the tunnel calibration MVD. This ratio avoided the complication of the uncertainty in tunnel LWC, and allowed a direct assessment of the relative spread of instrument results within the broad MVD envelope. One can first see from Figure 11 that all individual ratios were within ±20 % of the collective average response, with the exception of the lowest MVD point of N12mm416. However, again it is clear that there were systematic differences between the instruments. Focusing on MVDs larger than 50 µm, the Nevzorov ratios were lower than average by roughly 5-15%. The N8mm300 displayed relatively flat ratios relative to averages, whereas the N8mm416 and N12mm416 ratios increased somewhat with increasing MVD. N12mm416 did not appear to measure appreciably higher values than N8mm416 at the highest MVDs, as might have been expected due to its larger sample area, deeper depth, and expanded cone inner cavity. The ICDTWC and MWTWC behaved similarly. Their ratios were usually higher than the various Nevzorov sensors, but they also showed a distinct roll-off with increasing MVD relative to the collective average. The ROBTWC exhibited a fairly flat response relative to the collective average, with perhaps a small increase in relative response at the highest MVDs. The difference between the ROBTWC and the lowest response N8mm300 sensor at the 230 µm MVD test point, where a large number of tests were performed, was about a factor of 1.26. The largest spread in response for 50 µm MVD and above was at the 50 µm MVD test point, where there was roughly a scale factor of 1.43 between the MWTWC and N8mm300

Results from a second MVD sweep, performed at 100 $ms^{-1}$ and tunnel calibration LWC of 0.2 $gm^{-3}$, are shown in Figure 12. For these tests, a much smaller number of test points and repeats were performed due to limited tunnel time. Many of the same behaviors were observed as in Figure 11. All results were within ±20% of the average hot-wire results, and systematic differences between probes were observed. The ICDTWC and the ROBTWC readings were usually higher than the various Nevzorov readings. The MWTWC continued to show a roll-off relative to the other wires with increasing MVD. The ROBTWC, available only for the two highest MVD points, displayed the highest relative response for MVD greater than 178 µm, as in Figure 11. No clear pattern between the N12mm416 and N8mm416 was observed with this small number of points. Finally, the N8mm300 readings again were lower than those of the N8mm416. Note also that greater variability might be expected for this subtest due to the lower LWCs.

# Discussion

The question then arises as to how to interpret these results in terms of identifying a defensible LWC instrument or instruments for the CIRA IWT LWC calibration.

It has been concluded by others that present ice accretion methods for calibration yield lower LWCs than hot-wire TWC sensors in SLD conditions. The results of [10, 7] revealed that at 80 $ms^{-1}$, ratios of MWTWC to rotating cylinder LWC at the AIWT climbed to in excess of 1.5 at an MVD of 150 µm. Although not explicitly described in this article, those results were supported by our data. It is our contention that it is reasonable to conclude from this that the icing cylinders underestimate LWC in such conditions. There is in fact a precedent for implementing a hot wire tunnel LWC calibration. Ref. [6] found good agreement between icing blade and MWTWC measurements in low MVD conditions, and concluded that MWTWC measurements were superior in SLD and in high LWC conditions. Their study supported implementation of the change of the NASA IRT calibration standard from icing blade to the MWTWC.

Ref. [12] has recently independently reported on hot-wire comparisons from the Goodrich IWT in the USA, the Rail Tech Arsenal wind tunnel in Austria, and the Braunschweig IWT in Germany. They focused on comparison of Nevorov 8 mm and 12 mm TWC versus MW TWC measurements. The present study provided the opportunity to assess the same hot-wire designs, and the additional ICD and Robust probes, to further assess relative performance. It also provided comparative measurements collected from a different tunnel, one that is being used for the North American SLD Instrumentation Comparison Project [13], which includes cross referencing to the NASA IRT.

One first basic observation from the current study was that all results were contained within ±20% of the overall hot-wire average at the test point. If the average of all these devices represented the best estimate of the true LWC, this would represent the potential LWC errors expected over a community of different devices, within the limits of the conditions tested.

A second basic observation was that there were rather large systematic scale differences between different sensors that reached factors as high as roughly 1.43 in specific comparisons noted earlier. The Nevzorov probes almost always read lower than the MWTWC, ICDTWC, and ROBTWC. A similar underreading of the Nevzorov probes relative to the MWTWC at 85 $ms^{-1}$ was observed by [12] (their figure 5) at their lower MVDs, with a similar increase in Nevzorov relative response at higher MVDs. Multiple uncertainties that could contribute to inter-instrument scale factor differences are discussed in the next several paragraphs.

Tunnel blockage from the instruments themselves could cause changes in the LWC distribution specific to an instrument. As stated earlier, only one instrument was mounted in

the tunnel at a time as recommended in [7], from the bottom of the tunnel, and using a common mounting tube. The only blockage differences would be from the instruments themselves, which were all similar in size albeit not identical, or from different amounts of ice buildup during testing. Although it seems unlikely that these differences could cause the scale factor differences observed in this study, it cannot be completely ruled out. In the future, it may be prudent to perform accompanying icing cylinder measurements just ahead of the instrument for a subset of tests in order to quantify the importance of this effect. The possibility of a local flow affect specific to an instrument could be a generic problem affecting measurements at all facilities.

Day-to-day shifts in the tunnel-produced LWC for the same test point could have introduced inter-instrument scale factors during this study, because individual probes were sampled on different days, and any repeats from a specific probe used to estimate tunnel repeatability (Table 4) were also collected on the same day. One example of a day-to-day factor that could conceivably systematically introduce day-to-day LWC differences is tunnel relative humidity (RH), which could change the amount of evaporation between the nozzles and the test section. The RH in the wind tunnel was monitored during each test point via a Vaisala HMT337 humidity and temperature transmitter mounted in the settling chamber just upstream of the spray bars. Throughout the entire testing, the mean RH recorded during the spray activation was 84.7 %, and the day-to-day averages were between 82.1 and 87.4%. To provide an example of how the run-to-run variation in RH might have affected the LWC in the test section for a susceptible low-LWC, low MVD test point, the AIWT test condition of an MVD of 30 μm and LWC of 0.2 $gm^{-3}$ was simulated using the Arnold Engineering Development Center 1-Dimensional Multi-phase (AEDC 1DMP) code [21, 22]. Throughout the runs performed at this condition, the RH varied between 77% and 88%, over which the AEDC 1DMP code indicated that only a 2% difference in the LWC would be expected. At 20 μm MVD, the expected difference was 4%. So, although some individual points may have experienced departures from expected values, overall instrument-to-instrument scale factor differences attributable to day-to-day RH changes were certainly less than 4%, and most likely much lower. Furthermore, from accumulated experience, the AIWT staff considers that significant systematic day-to-day differences in LWC generation were unlikely.

The accuracy of inertial collision efficiencies could affect results. Appendix A has shown that the available efficiency estimates from the literature used mixed approaches, and there has been little assessment of their uncertainties. This would be particularly important for low-MVD cases, and bi-modal PSDs that were not included in the current study. Appendix A showed that applying the collision efficiency at the PSD bin diameter rather than the MVD could increase LWC by up to 4% for low MVDs, but this effect was less than 1% for the SLD cases of primary interest. But as efficiencies approached unity for all instruments with increasing MVD, these instrument scale differences persisted.

Each instrument has a sample area uncertainty that can introduce a scale factor difference between instruments. Applying estimated uncertainties of sensor length and width measurements provided by the manufacturer, the resulting lowest and highest calculated samples areas of the ROBTWC, ICDTWC, and MWTWC could lead to worst-case scale factor differences of about 1.05, 1.09, and 1.09 respectively. Length and width uncertainties could also, of course, work in opposite directions and drive that scale uncertainty down to much lower values. For the Nevzorov 8 and 12 mm TWC sensors, assuming a similar measurement uncertainty of 0.1 mm in sensor diameter, the corresponding high to low LWC scale factors would be about 1.05 and 1.03 respectively.

Instrument precision could also introduce scale factor differences. Response differences for different versions of the same sensor type, for example between N8mm416 and N8mm300, were observed during this study. This has also been observed before for MWTWC sensors, where scale differences of up to a factor of 1.15 have been observed [20]. While such inter-sensor differences for the same sensor type could again be due to sample area uncertainty, Ref. [20] attributed them to possible sensor irregularities or maintenance problems.

The apparent LWC vertical gradient measured by the ROBTWC during this study of between 5 and 15% from the tunnel center to 3.8 cm below the center was also considered as a possible contributor to scale differences. Sensors MWTWC, ICDTWC, ROBTWC, N8mm416, and N8mm300 were all tested at the tunnel center, and their comparisons to each other should not have been appreciably affected by such a gradient. However, sensor N12mm416 was tested 2.1 cm below the center, in an area of apparently higher LWC than the center. But this gradient was in the wrong direction to explain why the N12mm416 almost always read lower than the MWTWC, ICDTWC, and ROBTWC.

Finally, it is possible that icing on the mounting tubes and the sensors themselves may have affected results to varying degrees, albeit in a more random manner. More discussion on probe icing during these tests has been provided in [16], where the Nevzorov sensor vanes were found to occasionally collect considerable amounts of ice that could affect measurements.

Considering all of the issues above, it can easily be imagined that the observed scale factors between instrument LWCs may arise from a combination of such influences, which could potentially act across the full range of MVDs.

A more direct assessment of inter-instrument comparability can be obtained by using one instrument as a reference. Here we have chosen the ROBTWC, because it provided a high response in absolute terms, and a high response relative to others as MVD increased. Since only a limited number of measurements were taken with this instrument below 50 μm MVD, the SLD range was again the focus. Figure 13 displays the ratios of the various instrument readings to the ROBTWC, for the MVD sweep at 80 $ms^{-1}$ and a nominal tunnel LWC of 0.5 $gm^{-3}$. The ICDTWC and the MWTWC response rolled off relative to both the ROBTWC and the Nevzorov probes with increasing MVD. It is difficult to imagine how the latter probes could erroneously over-read at high MVD, particularly since the collision efficiencies at the high MVDs were essentially unity. We contend that the more reasonable argument is that the MWTWC and ICDTWC suffered from a higher rate of mass loss due to splashing and re-entrainment with increasing MVD than the ROBTWC. While the MWTWC did roll off

**FIGURE 13** As in Fig. 11, but for response relative to the SEA ROBTWC.

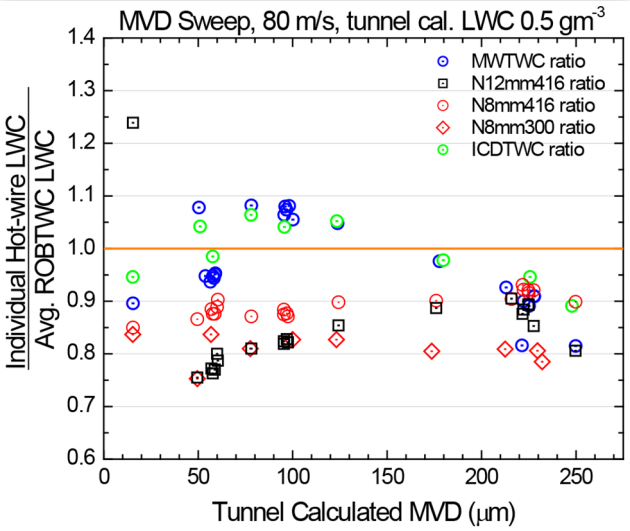


in both the 100 μm and 250 μm LWC sweeps (Figs. 8 and 9), consistent with Figure 13, the ICDTWC did not exhibit this roll-off relative to ROBTWC at 250 μm MVD and high LWC (Figure 9), an observation that warrants further testing and investigation. Second, note that both Nevzorov 8 mm readings were roughly a constant factor of the ROBTWC over the range of MVDs. The nearly constant scale factors for the Nevzorovs are interpreted as both having similar sensitivities to increasingly larger drops over this range of MVDs. The N12mm416 does show an increase in response relative to ROBTWC as MVD increases, at least to 230 μm MVD. It is not clear whether this is a definite increase in capture and evaporation efficiency. This sensor had the lowest inertial collision efficiency by a significant margin, and the response could be mathematically flattened relative to the ROBTWC simply by applying a lower collision efficiency at the lower MVDs (e.g. at 60 μm, changing the efficiency from 0.88 to 0.77). This rise in the N12mm416 to ROBTWC ratio is nevertheless an interesting observation that would appear to warrant a more dedicated test.

Overall, the results suggest that a similar sensitivity to large-droplet LWC response can be achieved for the conditions tested using the ROBTWC, the N8mm416, N8mm300, or the N12mm416 sensors, with roughly constant scale factors separating them. These are the sensors in Table 1 with the deepest capture volumes. The scale factors are however substantial, reaching a factor of about 1.25 between the ROBTWC and the N8mm300 sensor (Figure 13, ratio of approximately 1.0/0.8). This might approximately represent the worst-case calibration bias for European tunnels calibrated by these three different sensor choices under this range of conditions.

# Conclusions

Wind tunnel tests of the SEA Multi-Element probe (referred to in this study as the "multiwire"), the SEA Ice Crystal Detector, the SEA Robust probe, and two SkyPhysTech Research Nevzorov probes, one with a standard 8 mm conical TWC sensor, and the other with both 8 mm and 12 mm conical sensors, were performed in September 2020 at the National Research Council of Canada Altitude Icing Wind Tunnel. The tests focused on assessing the relative performance of these devices for tunnel LWC calibration in Supercooled Large Droplet conditions, to support the ICE GENESIS research program. A series of tests spanning a range of LWCs at 20, 100, and 230 μm MVDs was performed at 80 $ms^{-1}$. In addition, a range of MVDs between about 15 and 250 μm MVD were sampled at 80 $ms^{-1}$ and a roughly constant tunnel calibration LWC of 0.5 $gm^{-3}$. A more limited set was performed at 100 $ms^{-1}$ and a LWC of 0.2 $gm^{-3}$. Droplet volume distributions were fundamentally unimodal. Although the majority of testing was at LWC values greater than or equal to 0.5 $gm^{-3}$, higher than Appendix O requirements, the test points were chosen according to the practical limits of the facility, and to be compatible with test points of the independent SLD Instrumentation Collaboration study [13], which has conducted independent testing at the NASA IRT and the AIWT. Within the limits of the test conditions sampled, and subject to the accuracy of the calibration factors supplied by the manufacturers and sensor collision efficiencies currently available, the following conclusions were reached.

- Cylindrical sensors on the Nevzorov, Multiwire, and Ice Crystal Detector under-read LWC relative to their capture-volume sensors (i.e. TWC sensors: troughs, cones), as has been concluded from earlier studies, and were thus considered unsuitable for high MVD measurements.
- All instrument TWC sensor measurements were within ±20% of the average reading of those instruments for a given test point.
- Systematic differences between TWC sensors were observed, reaching up to about a factor of 1.43 for some conditions. Even the two geometrically equivalent Nevzorov 8 mm sensors on different Nevzorov systems displayed scale differences that could exceed a factor of 1.10. A good fraction of these systematic differences could be attributed to a combination of various effects, including but not limited to sample area measurement uncertainty estimated to reach 10%, collision efficiency uncertainty especially at the lower MVDs, and individual instrument precision. In order to further evaluate instrument scale factor differences, verifiable collision efficiency estimates based on common approaches, and a more detailed examination of sample area uncertainties would be primary topics on which to focus.
- Regarding the systematic differences, the Nevzorov TWC sensors usually measured lower than the SEA TWC sensors.
- Regarding the relative efficiency of sensors as MVD increased, and using the SEA Robust TWC sensor as a reference, the ratio of Multi-wire and Ice Crystal Detector TWC to the Robust TWC rolled off with increasing MVD, particularly above 125 μm. It is

contended here that it is reasonable to conclude that such roll-off is not an indication of over-reading by the Robust instrument, but rather due to more splashing at high MVD in the ICD and MW TWC sensors. There was comparable large droplet performance among the SEA Robust, Nevzorov 8mm, and Nevzorov 12 mm TWC sensors. The Nevzorov 8mm cone ratios were approximately flat with increasing MVD relative to the Robust TWC, albeit with the above noted scale factors differences. For example, similar response with increasing MVD would be expected between the Robust TWC and the Nevzorov 8 mm s.n. 300, but with the Robust TWC measuring about a factor of 1.25 higher.

- While TWC sensors collision efficiencies from published sources generally reached values of 0.95 or greater for droplet diameters of 50 µm or greater, those for the Nevzorov 12 mm TWC sensor were substantially lower, at about 0.83 at 50 µm, and only reaching 0.95 by about 100 µm MVD. This sensor did tend to have an increasing relative response relative to all others as MVD increased, but that result was dependent on the accuracy of those larger collection efficiency corrections. If correct, the measurements suggested about a 5% increase in response relative to the Robust TWC between 50 and 230 µm.
- If the true LWC in a tunnel were the average of all instruments tested, the ±20% noted above could represent the expected facility error if calibrated by one of these instruments. Worst case facility-to-facility differences could approach 40%.
- The Nevzorov probes had the disadvantage of sensor vane icing, which on occasion negatively affected measurements. For tunnel operations, this could also present substantial practical problems by requiring more frequent and costly shut-downs to de-ice.

# References


1. Biter, C.J., Dye, J.E., Huffman, D., and King, W.D., "The Dropsize Response of the CSIRO Liquid Water Probe," *J. Atmos. Oceanic Technol.* 4 (1987): 359-367.
2. Strapp, J.W., Oldenburg, J., Ide, R., Lilie, L. et al., "Wind Tunnel Measurements of the Response of Hot-Wire Liquid Water Content Instruments to Large Droplets," *J. Atmos. and Oceanic Technol.* 20 (2003): 791-806.
3. Baumgardner, D. et al., "Airborne Instruments to Measure Atmospheric Aerosol Particles, Clouds and Radiation: A Cook's Tour of Mature and Emerging Technology," *Atmospheric Res.* 102 (2011): 10-29, doi:10.1016/j.atmosres.2011.06.021.
4. Brenguier J.-L., Bachalo, W.D., Chuang, P.Y., Esposito, B.M. et al., "In Situ Measurements of Cloud and Precipitation Particles," in Wendish, M. and Brenguier, J.-L. (eds), *Airborne Measurements for Environmental Research: Methods and Instruments*, 1st edition (Wiley-VCH Verlag GmbH & Co. KGaA, 2013).
5. Lilie, L.E., Emery, E., Strapp, J.W., and Emery, J., "A Multiwire Hot-Wire Device for Measurement of Icing Severity, Total Water Content, Liquid Water Content, and Droplet Diameter," in *43rd AIAA Aerospace Sciences Meeting and Exhibit*, January 10-13, 2005, Reno, Nevada, AIAA 2005-859, 2005.
6. Steen, L., Ide, R., and Van Zante, J., "An Assessment of the Icing Blade and the SEA Multi-Element Sensor for Liquid Water Content Calibration of the NASA GRC Icing Research Tunnel," AIAA-2016-4051, 2016.
7. Clark, C., Orchard, D. et al., "Liquid Water Content Instrumentation Study and the NRC AIWT," in *SAE International, Conference on Icing*, Vienna, 2023.
8. Stallabrass, J., "LTR-LT-92 An Appraisal of the Single Rotating Cylinder Method of Liquid Water Content Measurement," NRC Laboratory Technical Report, Ottawa, 1978.
9. Ide, R.F. and Oldenburg, J.R., "Icing Cloud Calibration of the NASA Glenn Icing Research Tunnel," in *39th Aerospace Sciences Meeting and Exhibit*, Reno, NV, AIAA 2001-0234, 2001.
10. King-Steen, L., Strapp, J., Van Zante, J., and Orchard, D., "A Preliminary Study of Interfacility LWC Differences in Appendix C and Supercooled Large Droplet Conditions due to Calibration Instruments," AIAA-2021-2652, 2021.
11. Korolev, A.V., Strapp, J.W., Isaac, G.A., and Nevzorov, A.N., "The Nevzorov Airborne Hot-Wire LWC-TWC probe: Principle of Operation and Performance Characteristics," *J. Atmos. Oceanic Technol.* 15 (1998): 1495-1510.
12. Lucke, J. et al., "Icing Wind Tunnel Measurements of Supercooled Large Droplets Using the 12 mm Total Water Content Cone of the Nevzorov Probe," under review, Atmos. Meas. Tech., 2023.
13. Van Zante, J.F., Strapp, J.W., Esposito, B., Orchard, D. et al., "SLD Investigation in Icing Wind Tunnels – Investigation Overview," in *2021 AIAA Aviation Conference*, 2021.
14. Lilie, L.E., Sivo, C.P., and Bouley, D.B., "Description and Results for a Simple Ice Crystal Detection System for Airborne Applications," AIAA 2016–4058, 2016, https://doi.org/10.2514/6.2016-4058.
15. Strapp, J.W., MacLeod, J., and Lilie, L.E., "Calibration of Ice Water Content in a Wind Tunnel/Engine Test Cell Facility," in *15th International Conference on Clouds and Precipitation*, Cancun, Mexico, 2008.
16. Fleury, L., Bliankinshtein, N. et al., "Characterization of NRC Convair-580 Hotwire Probes Performance Using NRC AIWT," LTR-FRL-2021-0132, NRC Laboratory Technical Report, Ottawa, 2023.
17. Rigby, D.L., Struk, P.M., and Bidwell, C., "Simulation of Fluid Flow and Collection Efficiency for an SEA Multi-element Probe," in *6th AIAA Atmospheric and Space Environments Conference*, AIAA-2014-2752, 2014.
18. Wright, W.B., "User's Manual for the Improved NASA Lewis Ice Accretion Code LEWICE 1.6," NASA Contractor Rep. 198355, p. 96, 1995.
19. Wright, W.B., "User Manual for the NASA Glenn Ice Accretion Code LEWICE Version 2.0," NASA Contractor Rep. 1999-209409, p. 182, 1999.

20. King-Steen, L., Lilie, L., and Bouley, D., "An Examination of Causes of Multi-Wire Bias During SLD Instrumentation Testing in the IRT," AIAA-2021-2653, 2021.
21. Schulz, R.J., "Second Report for Research and Modelling of Water Particles in Adverse Weather Simulation Facilities," AEDC TASK Report 97-03.
22. Schulz, R.J., "A Model for Predicting Mixed-Phase Flow in Ground Test Facilities," in *37th AIAA Aerospace Sciences Meeting and Exhibit*, AIAA 99-0308, January 1999, Reno, NV.
23. Marongiu, P. Catalano, M., Amato, M., and Iaccarino, G., "UZEN: A Computational Tool Solving u-Rans Equations for Industrial Unsteady Applications," in *34th AIAA Fluid Dynamics Conference*, June 28–July 1, 2004.
24. Catalano, P. and Tognaccini, R., "Turbulence Modelling for Low Reynolds Number Flows," *AIAA Journal* 48 (2010): 1673-1685.
25. De Santis C., Catalano P., and Tognaccini R., "Model for Enhancing Turbulent Production in Laminar Separation Bubbles," *AIAA Journal*, vol. 60, pp. 473-487, Jan. 2022.
26. Catalano, P., De Rosa, D., Mele, B., Tognaccini, R. et al., "Performance Improvements of a Regional Aircraft by Riblets and Natural Laminar Flow," *Journal of Aircraft* 57, no. 1 (2020): 29-40.
27. Marino, A., Catalano, P., Marongiu, C., Peschke, P. et al., "Effect of High Voltage Pulsed DBD Plasma on the Aerodynamic Performances in Subsonic and Transonic Conditions," in *43rd AIAA Fluid Dynamics Conference*, June 24–June 27, 2013.
28. Catalano, P., Mele, B., and Tognaccini, R., "On the Implementation of a Turbulence Model for Low Reynolds Number Flows," *Computers and Fluids* 109 (2015): 67-71.
29. Catalano, P., "Application of a Hybrid RANS-LES Method to Free Shear Layers Flows," in *ASME International Mechanical Engineering Congress & Exposition, IMECE 2019*, November 11–14, 2019.
30. Iuliano, E., Brandi, V., Mingione, G., de Nicola, C. et al., "Water Impingement Prediction on Multi-element Airfoils by Means of Eulerian and Lagrangian Approach with Viscous and Inviscid Air Flow," in *44th AIAA Aerospace Sciences Meeting and Exhibit*, Reno, Nevada, AIAA paper 2006-1270, June 9–June 12, 2006.
31. Iuliano, E., Mingione, G., De Domenico, F., and de Nicola, C., "An Eulerian Approach to Three-Dimensional Droplet Impingement Simulation in Icing Environment," in *AIAA Giudance, Navigation, and Control Conference*, Toronto, Canada, AIAA paper 2010-7677, August 2–August 5, 2010.
32. Catalano, P. and Mele, B., "Modelling the Secondary Impingement of Supercooled Large Droplets in an Eulerial Environment," in *SAE International Conference on Icing*, June 20-22, 2023, Vienna, 23ICE-0079 Paper.
33. Langmuir, I. and Blodgett, K.B., "A Mathematical Investigation of Water Droplet Trajectories," *Collected Works of Irving Langmuir*, vol. 10 (Pergamon Press, 1946), 343-392.
34. Rigby, D.L. and Struk, P.M., "Simulation of Fluid Flow and Collection Efficiency at Low Stokes Number," AIAA 2020-2811, AIAA AVIATION 2020 FORUM, 2020.
35. Steen, L.E., Ide, R.F., Van Zante, J.F., and Acosta, W.J., "NASA Glenn Icing Research Tunnel: 2014 and 2015 Cloud Calibration Procedure and Results," NASA/TM—2015-218758, May 2015.
36. Nevzorov, A.N. and Shugaev, V.F., "Observations of the Initial Stage of Ice Phase Evolution in Supercooled Clouds," *Sov. Meteor. Hydro.* N8 (1992): 41-51.
37. Jeck, R.K., "Advances in the Characterization of Supercooled Clouds for Aircraft Icing Applications," FAA Report DOT/FAA/AR-07/4, November 2008.


## Contact Information

**Biagio M. Esposito**
CIRA - Centro Italiano Ricerche Aerospaziali
Via Maiorise 81043 – Capua (CE), Italy
b.esposito@cira.it

## Acknowledgments

This study was co-funded by CIRA-ProRA (Italian Aerospace Research Program), by the NRC within the GLAZEICE project, the NRC-AIWT, which provided the icing wind tunnel time slot for the experiment, and by the ICE-GENESIS project, the European Union's Horizon 2020 research and innovation program under grant agreement No 824310.

The authors would further like to thank Gislain Chevrette and Catherine Clark from NRC-AIWT, for providing technical support in the facility operation and technical information on tunnel data for the finalization of this manuscript. Finally, special thanks go to Mengistu Wolde (NRC FRL), and Christiane Voigt (DLR) for providing their expertise and instrumentation for the experiment.

## Definitions/Abbreviations

**AIWT** - Altitude Icing Wind Tunnel (NRC)

**AEDC 1DMP** - Arnold Engineering Development Center 1-Dimensional Multi-phase (AEDC 1DMP) model

**CIRA** - Centro Italiano Ricerche Aerospaziali

**D** - Sensor Diameter

**$D_c$** - Cylinder Diameter

**$d_{eff}$** - PSD effective diameter, ratio of third moment to second moment

**DLR** - German Aerospace Center

**$\varepsilon_{PSD}$** - Hot-wire inertial collision efficiency calculated from the PSD

**$\varepsilon_{MVD}$** - Hot-wire inertial collision efficiency calculated at the MVD

**FRL** - Flight Research Laboratory

**ICD** - Ice Crystal Detector (SEA)

**ICDTWC** - LWC measured by the ICD TWC sensor

**IRT** - Icing Research Tunnel

**L** - Sensor Length

**LWC** - Liquid Water Content

**MVD** - Median Volune Diameter

**MW** - SEA Multi-Wire probe (a.k.a. Multi Element Probe)

**N8mm416** - LWC measured by the Nevzorov 8 mm cone, SSN 416

**N8mm300** - LWC measured by the Nevzorov 8 mm cone, SSN 300

**N12mm416** - LWC measured by the Nevzorov 12 mm cone, SSN 416

**N12mm416** - LWC measured by the Nevzorov 12 mm cone, SSN 416

**NASA** - National Aeronautics and Space Administration

**NRC** - National Research Council of Canada

**PMS** - Particle Measuring Systems

**RC** - Rotating Cylinder

**RH** - Relative Humidity (tunnel)

**ROBTWC** - LWC measured by the Robust probe TWC sensor

**SA** - Sensor Sample Area

**SEA** - Science Engineering Associates

**σ** - Standard deviation

**SLD** - Supercooled Large Droplets

**SSN** - Sensor Serial Number

**W** - Sensor Width

**TWC** - LWC measured from a TWC sensor

**UZEN** - Unsteady Zonale Euler Navier-Stokes

# Appendix A. Inertial Collision Efficiencies

The inertial collision efficiencies described in this Appendix describe the expected fraction of upstream mass that impinges on the sensor sample area, determined by the trajectories of droplets and subject to their inertia and drag in the aerodynamic flow field around the sensor. The efficiencies do not include the effect of drop splashing and re-entrainment back into the flow field, which can greatly reduce overall collection and evaporation efficiency. The inertial collision efficiencies will hereafter be referred to simply as collision efficiencies.

The collision efficiencies used in the LWC calculation for the TWC and LWC sensors in this article are summarized below. There are differing levels of detail available for the various devices. We have attempted to use the best available information at the time of this analysis. For the SEA MW, Robust probe, and ICD, the efficiencies have been calculated at the average MVD value estimated from tunnel facility equations derived in the past from calibrations with the Malvern instrument. For the Nevzorov probes, a combination of calculations at the MVD and at estimated effective diameters has been used. Table A1 contains efficiencies for 80 and 100 $ms^{-1}$ for each sensor using the parameterizations or assumptions listed below, sometimes from more than one source. The specific values used in this article are highlighted with an asterisk in the column header. All sensors have calculated collision efficiencies of 0.95 or greater for drop diameters greater than about 50 μm, with the exception of the Nevzorov 12 mm TWC sensor, suggesting that efficiency uncertainty is not a major issue for comparisons in the SLD conditions of this report. The effect of discrete PSD calculations on collision efficiencies is described late in this appendix.

# New CIRA Numerical Simulations

CIRA has recently completed two-dimensional numerical simulations of the Robust probe body and TWC sensor, and is currently performing corresponding simulations for the ICD TWC and LWC sensors. A description of the simulation algorithm follows.

The method computes the aerodynamic flow field around the body and sensor, and then calculates drop particle trajectories in the flow field to estimate the collision efficiency. The CIRA-developed flow solver UZEN (Unsteady Zonale Euler Navier-Stokes) [23] was used for the first step. UZEN solves the compressible Navier-Stokes equations based on a multi-block structured approach, and is normally used for simulating steady and unsteady flows around complex aeronautical models. Evidence of its efficacy has been provided through reproduction of flows involving some peculiar phenomena [24, 25] and for complex devices [26, 27]. The spatial discretization in UZEN consists of a central finite-volume formulation with explicit blended $2^{nd}$ and $4^{th}$ order artificial dissipation. A dual-time stepping technique is employed for accurate simulations. The pseudo-time integration uses an explicit hybrid multistage Runge-Kutta scheme. Classical convergence acceleration techniques, such as local time stepping and implicit residual smoothing, are available together with a multigrid algorithm. Turbulence is modelled by either algebraic or transport equation models [28], and hybrid RANS-LES methods are also employed [29].

The impingement of the water droplets was then calculated using the Imp3D [30, 31] method developed by CIRA. The Imp3D code uses a Eulerian approach to solve the partial differential equations, dependent on the drop volume fraction, velocity and temperature, that govern the movement of the water drops through the flow field. Several bouncing and splashing models are implemented as well as shattering models in case of ice crystals. Models derived from the literature account for the effect

**TABLE A1** Approximate inertial collision efficiencies for nominal test points considered for this study.

| | | | SEA Multiwire | | | Robust | | ICD | | Nevzorov | | | | |
|---|---|---|---|---|---|---|---|---|---|---|---|---|---|---|
| ε calc. used (*) | | | * | * | * | * | | * | * | * | | * | | * |
| ε calculated at ---> | | | MVD | MVD | MVD | MVD | MVD | MVD | MVD | *deff* | *deff* | MVD | *deff* | MVD |
| Vel. ($ms^{-1}$) | MVD (μm) | deff (μm) | MWTWC Refs. [17,6] | MWLWC021 0.533 mm, Refs.[17,6] | MWLWC083 2.11 mm, Refs.[17,6] | ROBTWC (CIRA, this article) | ROB-TWC Ref. [34] | ICDTWC (see text) | ICDLWC 2.4 mm, (see text) | N12mm-TWC Refs. [11,12] | N8mm-TWC Ref. [11] | N8mm-TWC Ref. [2] | NLWC Ref. [11] | NLWC Ref. [33] |
| 80 | 15 | 12.8 | 0.904 | 0.933 | 0.885 | 0.997 | 0.862 | 1.0 | 1.0 | 0.346 | 0.744 | 0.831 | 0.983 | 0.951 |
| 80 | 20 | 17.0 | 0.931 | 0.950 | 0.918 | 0.998 | 0.909 | 1.0 | 1.0 | 0.483 | 0.837 | 0.873 | 0.990 | 0.966 |
| 80 | 28 | 23.8 | 0.953 | 0.965 | 0.946 | 0.999 | 0.948 | 1.0 | 1.0 | 0.646 | 0.910 | 0.909 | 0.995 | 0.978 |
| 80 | 40 | 34.0 | 0.970 | 0.977 | 0.966 | 0.999 | 0.975 | 1.0 | 1.0 | 0.789 | 0.954 | 0.937 | 0.998 | 0.986 |
| 80 | 50 | 39.2 | 0.978 | 0.983 | 0.975 | 1.000 | 0.986 | 1.0 | 1.0 | 0.832 | 0.965 | 0.949 | 0.998 | 0.990 |
| 80 | 57 | 48.5 | 0.982 | 0.986 | 0.980 | 1.000 | 0.991 | 1.0 | 1.0 | 0.884 | 0.977 | 0.955 | 0.999 | 0.992 |
| 80 | 78 | 61.2 | 0.989 | 0.992 | 0.988 | 1.000 | 0.999 | 1.0 | 1.0 | 0.924 | 0.985 | 0.967 | 0.999 | 0.994 |
| 80 | 100 | 78.4 | 0.994 | 0.995 | 0.994 | 1.000 | 1.002 | 1.0 | 1.0 | 0.952 | 0.991 | 0.975 | 1.000 | 0.996 |
| 80 | 125 | 98.0 | 0.997 | 0.998 | 0.997 | 1.000 | 1.003 | 1.0 | 1.0 | 0.969 | 0.994 | 0.980 | 1.000 | 0.997 |
| 80 | 175 | 137.2 | 1.001 | 1.001 | 1.001 | 1.000 | 1.001 | 1.0 | 1.0 | 0.984 | 0.997 | 0.985 | 1.000 | 0.998 |
| 80 | 210 | 164.6 | 1.002 | 1.002 | 1.003 | 1.000 | 0.999 | 1.0 | 1.0 | 0.989 | 0.998 | 0.988 | 1.000 | 0.998 |
| 80 | 230 | 180.3 | 1.003 | 1.003 | 1.003 | 1.000 | 0.998 | 1.0 | 1.0 | 0.991 | 0.998 | 0.989 | 1.000 | 0.999 |
| 80 | 250 | 196.0 | 1.003 | 1.004 | 1.003 | 1.000 | 0.996 | 1.0 | 1.0 | 0.992 | 0.999 | 0.990 | 1.000 | 0.999 |
| 100 | 30 | 25.5 | 0.961 | 0.971 | 0.955 | 0.999 | 0.960 | 1.0 | 1.0 | 0.677 | 0.920 | 0.923 | 0.996 | 0.982 |
| 100 | 178 | 139.6 | 1.001 | 1.001 | 1.002 | 1.000 | 1.000 | 1.0 | 1.0 | 0.984 | 0.997 | 0.987 | 1.000 | 0.998 |
| 100 | 235 | 184.2 | 1.003 | 1.003 | 1.004 | 1.000 | 0.996 | 1.0 | 1.0 | 0.991 | 0.998 | 0.990 | 1.000 | 0.999 |

The efficiencies that were actually used are identified with an asterisk in the second row. Efficiencies were either evaluated at the MVD calculated from tunnel calibration equations, or the effective diameter deff estimated from it, as indicated in the third row of the table.

of particle shape on heat transfer. The effect of phase change (evaporation and melting) is simulated with evaporation models that compute the rate change of the particle mass as function of the Sherwood number. The melting process is also incorporated. Impingement caused by large droplets impacting the body and re-injecting secondary drops into the flow field has recently been added to the code [32]. The spatial discretization in Imp3D is also based on a finite-volume approach. The convective terms are solved through centered numerical derivatives with the addition of adaptive artificial dissipation. In particular, third-order diffusive terms are added everywhere to prevent numerical instabilities, while first order terms are needed to capture flow discontinuities. A properly designed numerical sensor, based on the water volume fraction, automatically switches the dissipation order when strong gradients are encountered. The time integration is performed by the Runge-Kutta algorithm and the local time-stepping procedure is applied to speed-up the convergence towards a steady state.

The impingement code was used to produce local mass fluxes along the LWC or TWC sensor surfaces. The fluxes were then integrated over the sensor surface, and ratioed to the water flux in a plane ahead of the exposed sensor area, producing the sensor collision efficiency.

# Cylindrical Collision Efficiencies from Ref. [33]

Langmuir and Blodgett (1946) [33] collision efficiencies for droplets at the MVD values of the test points are given in Table A2. These are provided as reference for comparison to the more complex treatments below. The 0.533, 2.0, 2.11, 2.39, and 2.40 cylinder diameters are those of the Multiwire "021", Nevzorov, Multiwire "083", and ICD LWC sensors, and the NRC rotating icing cylinder used for lower MVDs.

# SEA Robust Probe

Two options for Robust TWC efficiencies were considered. First, new CIRA numerical simulations, as described above, were used to estimate efficiency of the Robust TWC sensor for the range of test conditions. A two-dimensional representation of the sensor was used. Second, efficiencies were calculated using the equations of [34], derived from three-dimensional numerical simulations. Although the latter parameterizations were derived for ice particles of density 0.917 $gcm^{-3}$, there was nothing specific in the methodology that would preclude applying their equations to water droplets (Rigby, personal communication).

**TABLE A2** Calculated Langmuir and Blodgett (1946) [33] collision efficiencies for simple cylinders for the MVD Sweep test points at 80 and 100 $ms^{-1}$, for comparison to cylindrical sensors in Table 1 when appropriate (pressure=100 KPa, temperature = -5 C).

| | | Cylinder Dia. | | | | |
|---|---|---|---|---|---|---|
| Vel. ($ms^{-1}$) | Drop Dia (μm) | 0.533 mm | 2.0 mm | 2.11 mm | 2.39 mm | 2.40 mm |
| 80 | 15 | 0.986 | 0.951 | 0.948 | 0.941 | 0.941 |
| 80 | 20 | 0.991 | 0.966 | 0.964 | 0.960 | 0.959 |
| 80 | 28 | 0.994 | 0.978 | 0.977 | 0.974 | 0.974 |
| 80 | 40 | 0.996 | 0.986 | 0.986 | 0.984 | 0.984 |
| 80 | 50 | 0.997 | 0.990 | 0.989 | 0.988 | 0.988 |
| 80 | 57 | 0.998 | 0.992 | 0.991 | 0.990 | 0.990 |
| 80 | 78 | 0.999 | 0.994 | 0.994 | 0.993 | 0.993 |
| 80 | 100 | 0.999 | 0.996 | 0.996 | 0.995 | 0.995 |
| 80 | 125 | 0.999 | 0.997 | 0.997 | 0.996 | 0.996 |
| 80 | 175 | 0.999 | 0.998 | 0.998 | 0.998 | 0.998 |
| 80 | 210 | 1.000 | 0.998 | 0.998 | 0.998 | 0.998 |
| 80 | 230 | 1.000 | 0.999 | 0.999 | 0.998 | 0.998 |
| 80 | 250 | 1.000 | 0.999 | 0.999 | 0.998 | 0.998 |
| 100 | 30 | 0.995 | 0.982 | 0.981 | 0.978 | 0.978 |
| 100 | 178 | 1.000 | 0.998 | 0.998 | 0.998 | 0.998 |
| 100 | 235 | 1.000 | 0.999 | 0.999 | 0.999 | 0.999 |

The diameters of the MW LWC "021", MW LWC "083", Nevzorov LWC, ICD LWC, and NRC icing cylinder are 0.533, 2.11, 2.0, 2.39 and 2.40 mm respectively.

Results of both simulations are provided for the test point sizes (MVDs) in Table A1. The comparisons of the simulations are preliminary, and require further investigation, but they do show that efficiencies for both simulations exceeded 0.97 for diameters greater than 40 μm. Therefore, for the higher MVD SLD test points, either efficiency algorithm would produce nearly equivalent results. However, for the 28 μm and lower test points, the CIRA simulations produced significantly higher efficiencies. For example, at 20 μm, the Ref. [32] and CIRA efficiencies are 0.91 and 0.998 respectively. As shown in Appendix B, comparisons of the CIRA efficiency-corrected Robust LWC during the 20 μm MVD LWC sweeps agreed better with icing cylinder measurements taken during the wind tunnel testing, and for this reason, it was decided to use the CIRA efficiencies for the SEA Robust probe calculations in this article. Nevertheless, it is acknowledged that further investigations of the discrepancy between CIRA and Ref. [34] efficiencies should be pursued.

## SEA Ice Crystal Detector

To date, there has been no reported study of water drop collision efficiencies for the SEA ICD TWC and LWC sensors. Furthermore, CIRA numerical simulations described above were not completed for the ICD in time for this article. In the absence of any other reliable information, the efficiencies for the ICD TWC and LWC sensors have been assumed to be 1.0 for all test points of this study. Given that the Robust probe TWC housing is approximately the same dimensions as that of the ICD, with only the width of the ICD TWC sensor being smaller, and given that the CIRA Robust TWC collision efficiencies exceed 0.99 for diameters larger than about 7 μm, the assumption of unit collision efficiency for the ICD TWC may in fact be reasonable for the test conditions of Table A1. As for the ICD LWC sensor, it is the same width as the TWC sensor, and is located immediately below at the center leading edge of the housing. It was so designed to provide similar liquid response in Appendix C conditions. Some support for equivalent ICD TWC and LWC sensor collision efficiencies comes from the nearly identical pre-efficiency corrected water contents calculated during LWC sweeps at 20 μm MVD. The unit efficiencies for the ICD LWC and TWC sensors will be revisited upon completion of the CIRA numerical simulations.

## SEA Multi-Wire Probe

Collision efficiencies for the three wires of the MW probe have been calculated according to Ref. [6], originally derived from LEWICE3D particle trajectory code coupled with a three-dimensional flow field analysis [17]. Some of the details of the final calibration equations which describe efficiency as a function of MVD and airspeed, are specific to the NASA IRT PSDs, but were nevertheless used in this article assuming a similar character to the AIWT PSDs. More detail can be found in Refs. [6]

and [35]. Table A1 lists these efficiencies at the MVDs of the test points used in this article. For reference, at the low MVDs, the LWC sensor efficiencies are lower than the Table A2 values of Ref. [33], likely due to the effect of the sample tube surrounding the wires that is not taken into account in the simpler Ref. [33] calculations.

# Nevzorov Sensor Vanes: Cylindrical LWC, and Conical 8 mm and 12 mm Diameter TWC Sensors

Ref. [11] provided the following relationship for collision efficiency of the standard Nevozorov sensor vane LWC and TWC sensors as a function of the effective diameter: $\varepsilon=d_{eff}^2/(d_{eff}^2+d_0^2)$, where the $d_{eff}$ was defined as the ratio of the third to second moments of the PSD, and where $d_0$ was a constant specific to the element geometry. Ref. [11] recommended $d_0$ values of 7.5 and 1.7 μm for the 8 mm conical TWC sensor and 2 mm LWC sensors respectively, for an airspeed of 100-150 $ms^{-1}$, and referred the reader to [36] for more detail. The 12 mm conical TWC sensor incorporates a larger diameter and a deeper cone with a special design ostensibly to increase the efficiency of capture and retention of large droplets. For the efficiency of this sensor, the approach of Ref. [12] was adopted, which uses the Ref. [11] equation above, with a $d_0$ value of 17.6 at 85 $ms^{-1}$ derived by [12]. No adjustments to $d_0$ were made for the 80 and 100 $ms^{-1}$ test conditions.

In order to apply the manufacturer's collision efficiency algorithm, $d_{eff}$ values were estimated from the NRC SprayTek Malvern data collected during the tests of 24-Sep-2020, and then compared to MVD values. The results were well correlated. For the small-caps nozzles used for MVDs lower than about 60 μm, a linear regression through the origin yielded $d_{eff}=0.850\ MVD$, with $r^2=0.985$ and a standard slope error of 0.011. For the large-caps nozzles used for higher MVDs, the regression yielded $d_{eff}=0.784\ MVD$ with $r^2=0.948$ and a standard slope error of 0.016. Since estimates of the MVDs for each test point were available from the AIWT tunnel calibration equations, but PSDs from which $d_{eff}$ values could be computed were typically not available, these MVDs were averaged over the test point period, and then converted to $d_{eff}$ values using the equations above.

A second option for the efficiency of the 8 mm TWC sensor has been provided in [2]. For that article, NASA performed LEWICE2D [18, 19] calculations of a two-dimensional representation of the Nevzorov 8 mm TWC sensor, and derived a simplified efficiency parameterization of the form $\varepsilon=(1-(3.5-0.012*V)/d_{drop})$, where V was the air velocity in $ms^{-1}$, and $d_{drop}$ was the drop diameter in μm. Although some details of this parameterization are no longer traceable, it is known that it was computed for wind tunnel conditions between 67 and 100 $ms^{-1}$, and temperatures between 0 and -10 C, and therefore is compatible with the range of conditions of the current wind tunnel tests. The parameterization does not apply to the 12 mm TWC sensor. Table A1 includes 8 mm TWC efficiencies for the two options noted above. The manufacturer's efficiencies based on $d_{eff}$ are generally lower for MVDs less than about 28 μm, and higher above this MVD. Since the former were quoted for velocities in the 100-150 $ms^{-1}$ range, and efficiency generally increases with velocity, for this article the efficiencies of [2] were used.

For the Nevzorov LWC sensor, the efficiencies of [11] and [33] were both considered, and are both listed in Table A1. Both exceed 0.99 for diameters greater than 50 μm, but the efficiencies of [33] are increasingly lower as diameters decrease. At 20 μm, the Ref. [33] and [11] efficiencies are 0.966 and 0.990 respectively. Again, due to the higher airspeed range quoted by [11], the efficiencies of [33] were used for this article.

In summary, the efficiencies of [11, 12], [2], and [33] were used for the 12 mm TWC, 8 mm TWC, and the LWC sensors respectively.

# Discrete PSD Efficiencies versus Efficiencies at the MVD

Ideally, the collision efficiency versus diameter should be applied to the actual diameter intervals of the measured PSD. Since PSDs were not available for each test condition, but estimates of MVD for individual test point run were available from the tunnel MVD calibration equations and nozzle and tunnel parameters, hot-wire collision efficiencies were calculated at the specific MVD calculated for each run. On 24-Sep-2020, the Malvern was operated for all test points, providing the opportunity to compare the effective efficiencies based on a discrete PSD calculation, and the efficiency calculated at the MVD. The PSD-based efficiency $\varepsilon_{PSD}$ was defined as the following:

$$\varepsilon_{PSD}=\frac{\sum V(i)\varepsilon(i)}{\sum V(i)}$$

where $V(i)$ was the volume fraction in bin i and $\varepsilon(i)$ was the hot wire efficiency of the diameter associated with bin i. The sum of the V(i) values was unity by definition.

Ratios of $\varepsilon_{PSD}$ to $\varepsilon_{MVD}$ are shown in Fig. A1 for the MW, Nevzorov 8 mm cone, and Robust TWC sensors. The ICD TWC sensor, not included, likely would have similar results to the Robust TWC sensor. All $\varepsilon_{PSD}$ values for each TWC sensor were

**FIGURE A1** Ratio of effective efficiency of hot-wire TWC sensors: integrated over the PSD ($\varepsilon_{PSD}$) to calculated at the MVD ($\varepsilon_{MVD}$). Data were derived from Malvern measurements on 24-Sep-2020, and hot-wire efficiencies in this appendix.

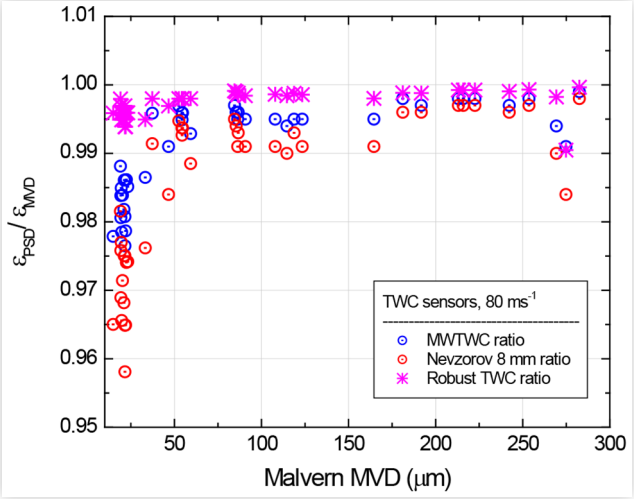


**FIGURE A2** As in Fig. A1, but for cylindrical hot-wire LWC sensors.

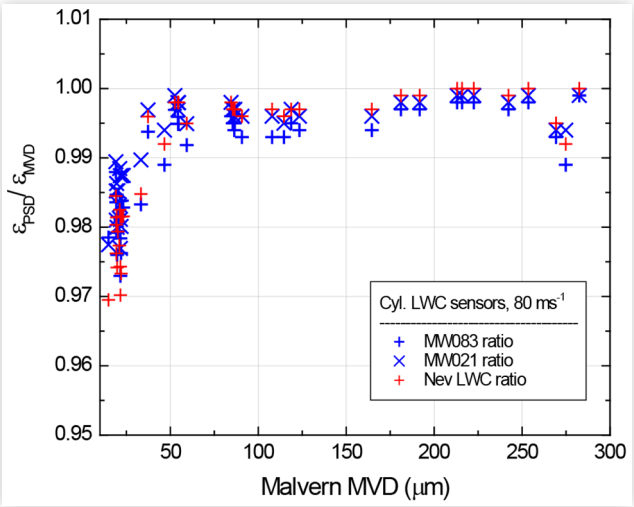


lower than that calculated at the MVD. Above approximately 50 μm MVD, all $\varepsilon_{MVD}$ values for all sensors were within about 1% of $\varepsilon_{PSD}$. For test points with MVDs less than or equal to 50 μm MVD, the Robust TWC performed best due to its higher efficiencies, with $\varepsilon_{MVD}$ values remaining within 1% of $\varepsilon_{PSD}$. In this MVD range, the MWTWC and Nevzorov 8 mm cone $\varepsilon_{PSD}$ reached about 2.5% and 4% lower than $\varepsilon_{MVD}$ at about 20 μm MVD. A corresponding plot for the cylindrical LWC sensors (MW 2.1 mm, MW 0.53 mm, and Nevzorov 2.0 mm) is given in Figure A2. Similar results were found. Above 50 μm, $\varepsilon_{PSD}$ values were as much as 1% lower than $\varepsilon_{MVD.}$ Below 50 μm MVD, $\varepsilon_{PSD}$ values were as much as about 3% lower.

# Appendix B. Cylindrical LWC Sensor Results

The results of the cylindrical LWC sensor measurements from the Nevzorov sensor s.n. 300, Nevzorov sensor s.n. 416, the two SEA MW s.n. 2086 LWC sensors, and the ICD s.n. 416, are documented in this Appendix. Since the straightforward conclusion is that the results all substantially drop off with increasing MVD relative to those of the TWC sensors, it was decided to separate their results from the main body of the article to simplify the discussion of SLD measurement there. Table B1 contains the details on the length and diameters of each sensor. All LWC calculations in this appendix incorporate the inertial collision efficiencies described in Appendix A.

**TABLE B1** Cylinder Diameter ($D_c$), length (L), sample area (SA), of the LWC sensing elements in this study

| Sensor | Serial Number | $D_c$ (mm) | L (mm) | SA ($mm^2$) |
|---|---|---|---|---|
| MW | 2086 | 0.533 | 21.89 | 11.67 |
| MW | 2086 | 2.108 | 21.03 | 44.33 |
| Nevzorov | 300 | 2.0 | 16.2 | 32.4 |
| Nevzorov | 416 | 2.0 | 16.3 | 32.6 |
| ICD | 4005 | 2.388 | 10.211 | 24.38 |

# LWC Sweeps at 20 μm MVD

Just prior to the instrument testing, spot checks were performed with the NRC AIWT rotating cylinder (RC), to check the continuing accuracy of the tunnel LWC calibration equations. The 20 μm MVD is a commonly used test condition and is close that observed in the majority of Appendix C clouds [35]. It was also suspected that splashing and re-entrainment of large droplets may not be occurring to a significant degree on the RC at this MVD[1]. Accordingly, it is contended here that the 20 μm MVD test points represent a benchmark for assessing response of the instruments under one of the least complicated and often used test conditions.

Figure B1 shows results of the 80 $ms^{-1}$ LWC sweeps at approximately 20 μm MVD. Collision efficiencies used in the calculations are summarized in the legend, along with linear regression slopes through the origin. It is evident that there were some scale factor differences in the response of the various sensors. The RC results approximately reproduced the tunnel equation LWC as expected, and were approximately the same as results from the ICDLWC. The two NLWC sensors measured about 0.76 and 0.81 of the tunnel and RC measurements. Ref. [11] compared Particle Measuring Systems (PMS) King probe (a ~2 mm diameter cylindrical hot wire LWC device [1]) and Nevzorov LWC and TWC measurements in cumulus congestus reaching greater than 2 $gm^{-3}$, and similarly found ~15% lower readings from the Nevzorovs, concluding that sample area uncertainty could have contributed to the difference. In Figure B1, the MWLWC with the 0.533 mm sensor had the lowest LWC response, and a possible roll-off with increasing LWC. With its high collision efficiency of about 0.95 for these conditions, computed with the three-dimensional numerical model of the MW (Appendix A), there is little possibility that the low results were low due to inertial efficiency uncertainty. The most likely explanation is that even at 20 μm MVD, a certain amount of particle splashing and re-entrainment may have contributed to lower overall collection and evaporation efficiency, and it was worst for the smallest diameter sensor. Figure B2 shows the same data, but this time plotting the cylindrical LWC sensor results versus the TWC sensor results from the same instrument, rather than the tunnel calibration LWC. It is evident that LWC measurements of each instrument were either approximately equal to, or lower than the same instrument's TWC measurement. Since this was a consistent observation for all instruments, this supported the contention above that there may be some loss of LWC by most of the cylindrical sensors even at this relatively low MVD.

**FIGURE B1** Cylindrical LWC sensor results for the 80 $ms^{-1}$, 20 μm MVD LWC sweeps. Approximate collision efficiencies are included in the legend, as are the linear regression slopes though the origin. Rotating icing cylinder measurements are also shown.

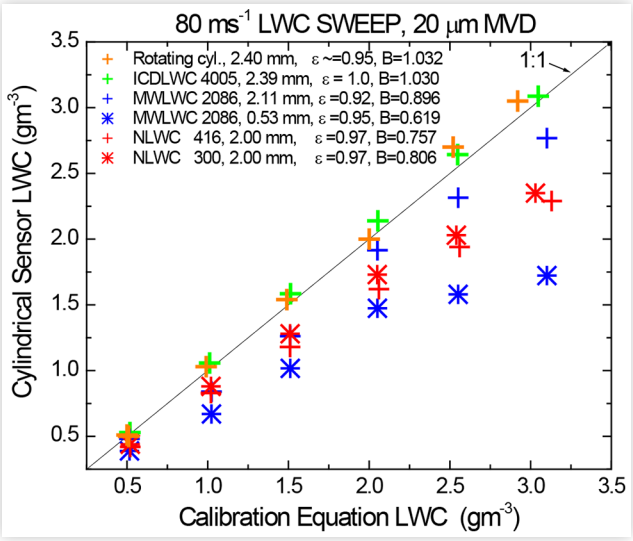


[1] The rotating cylinder used for 20 μm MVD has a diameter of 2.4 mm, and an approximate collision efficiency of 0.95.

**FIGURE B2** As in Fig. B1, but with cylindrical LWC measurements plotted against the same instrument's simultaneous TWC sensor measurement. For the Nevzorov SN 416, the 8 mm TWC sensor was chosen as reference rather than the 12 mm sensor.

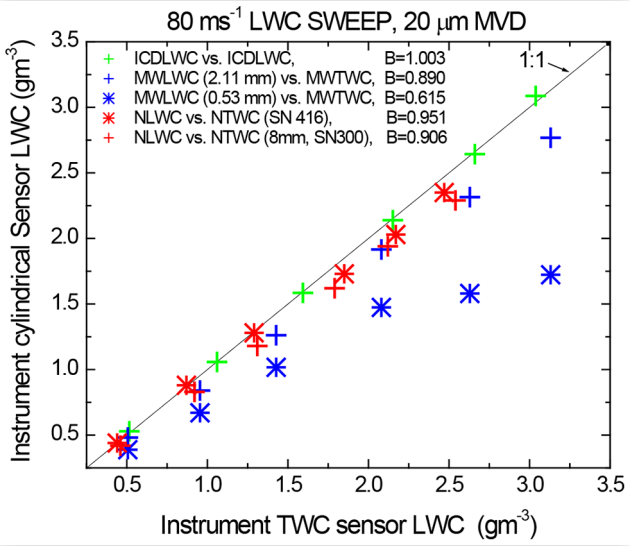


Figure B3 display ratios of simultaneous measurements of the cylindrical LWC sensors to the TWC sensors from the same instrument at 80 $ms^{-1}$, but this time at a tunnel calibration LWC of 0.5 $gm^{-3}$, and over a wide range of MVDs. All cylindrical LWC measurements dropped off with MVD relative to the TWC measurement, as has been observed in other studies. The smallest variation in ratios was for the SEA ICD, and the largest was for the 0.533 diameter MW LWC sensor. Figure B4 displays the same information at 100 $ms^{-1}$ and a tunnel calibration LWC of 0.2 $gm^{-3}$. Note that this data subset includes only three test point MVDs. Comparing Figures B2 and B3, the roll-off in the LWC sensors was quite similar at 80 and 100 $ms^{-1}$.

The most important conclusion from Figures B1-B4 is that all the LWC sensors had a decreasing response with increasing MVD relative to the TWC sensors of the same instrument. This was even detectable for some of the LWC sensors at 20 μm MVD, and was likely due to droplet splashing and re-entrainment that became more important as MVD increased. The TWC sensors therefore provide a superior measurement in SLD conditions. Nevertheless, for very low MVDs and low velocities, LWC sensors may provide better measurements due to the typically larger diameters and thus lower collision efficiency of TWC sensors.

**FIGURE B3** Ratio of instrument LWC measurement to simultaneous TWC element measurement from same instrument, at 80 ms-1 and a tunnel calibration LWC of 0.5 $gm^{-3}$.

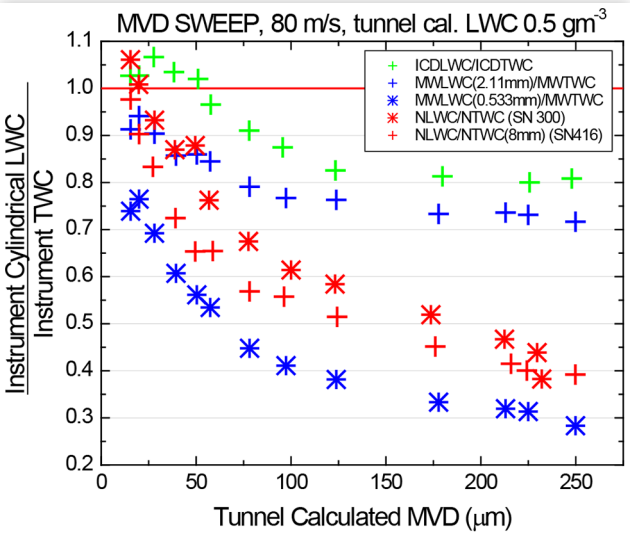

**FIGURE B4** As in Figure B3, but for the MVD sweep at 100 ms-[1], and a tunnel calibration LWC of 0.2 gm-[3].

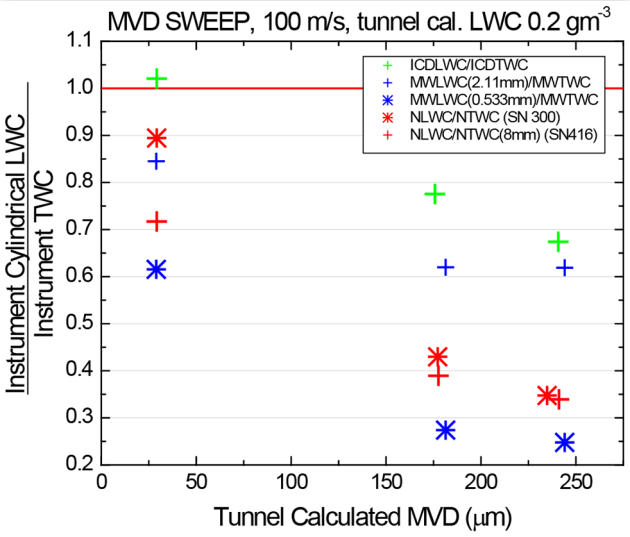




ISSN 0148-7191